Role of Aromatic Side Chains in the Binding of Volatile General Anesthetics to a Four-α-Helix Bundle†

Gavin A. Manderson‡ and Jonas S. Johansson*,‡

Department of Anesthesia and the Johnson Research Foundation, University of Pennsylvania, Philadelphia, Pennsylvania, 19104

Received December 19, 2001; Revised Manuscript Received January 30, 2002

ABSTRACT: Currently, the mechanism by which anesthesia occurs is thought to involve the direct binding of inhaled anesthetics to ligand-gated ion channels. This hypothesis is being studied using four-α-helix bundles as model systems for the transmembrane domains of the natural "receptor" proteins. This study concerns the role in anesthetic binding played by aromatic side chains in the binding cavity of a four-α-helix bundle designed to assume a Rop-like fold. Specifically, the effect of the substitution W15Y on bundle structure, stability, and anesthetic binding energetics was investigated. No appreciable effect of substituting W for Y on the secondary structure or the thermodynamic stability of the four-α-helix bundle was identified. However, the substitution W15Y resulted in about 6- and 3-fold decreases in halothane and chloroform binding affinities, respectively. This effect may reflect weaker dipole−aromatic quadrupole interactions between the aromatic side chain and the anesthetic in the tyrosine-containing species, which possesses the smaller aromatic ring system. For these anesthetic binding proteins, this class of interaction occurs when the permanent nonspherical distribution of electrons in the aromatic ring systems interact with the weakly acidic CH group of the anesthetics.

The mode of action of inhalational anesthetics is poorly understood (*1*, *2*), although several studies concerning their interactions with proteins, for example luciferase (*1*, *3*, *4*), exist. However, the specific in vivo targets of inhalational anesthetics, though currently unknown, are thought to be ligand-gated ion channels and neurotransmitter receptors in the central nervous system (*1*, *5*). To gain an understanding of how these interactions cause anesthesia, structural information describing how anesthetics bind to their receptor proteins is required. Yet, at present, determining the high-resolution structures of intact membrane-bound receptor proteins, for example, the nicotinic acetylcholine receptor (*6*) or similar receptors which may bind anesthetics, has proven to be unsuccessful. In addition, binding studies of volatile anesthetics to membrane proteins have been limited to two naturally pure preparations: the *Torpedo nobiliana* nicotinic acetylcholine receptor (*7*) and bovine rhodopsin (*8*).

To circumvent these problems, the structures of putative anesthetic receptors and anesthetic binding systems are currently being studied using water-soluble synthetic peptides that fold to form the common antiparallel α-helical bundle motif, scaled down models that presumably mimic the structures of the in vivo receptors. For example, the four-α-helix bundle is a prominent structural feature of the potassium channel from *Streptomyces lividans* (*9*) and bacterial photosynthetic reaction centers (*10*). In their work with synthetic peptides, Johansson et al. use four-α-helix bundles similar to those of Gibney and co-workers (*11*−*13*), which fold to form a Rop-like four-α-helix bundle structure.

Another problem encountered in the study of anesthetic binding by their in vivo receptors is that this type of interaction is relatively weak, with K_d values in the high μM and low mM range (*1*). However, techniques such as direct photoaffinity labeling and fluorescence quenching have proven successful in determining binding affinities in the model systems of Johansson et al. (*14*). This group found that the four-α-helix bundle $(A\alpha_2)_2$[1] (*15*) binds halothane in the internal cavity with a $K_d = 710$ μM, as determined by the quenching of W^{15} fluorescence. Photolabeling revealed that [^{14}C]halothane was incorporated at a stoichiometry of anesthetic/four-α-helix bundle of 1:1 (*14*). Microsequencing results showed that most counts were associated with residue^{15}, indicating that halothane interacts directly with the side chain of W^{15}. The K_d value is comparable to the EC_{50} value for halothane in humans, which is 250 μM (*1*), suggesting that, in both systems, the anesthetic is interacting with binding sites of comparable structure. Corroboration of the structural information obtained using the techniques of direct photoaffinity labeling and fluorescence quenching should be possible by measuring the changes in binding affinities that occur as a consequence of amino acid substitutions.

† This work was supported by the National Institutes of Health (Grant GM55876).

* Corresponding author. Phone: (215) 349-5472. Fax: (215) 349-5078. E-mail: JohanssJ@uphs.upenn.edu.

‡ Department of Anesthesia.

[1] Abbreviations: $(A\alpha_2)_2$, four-α-helix bundle; W15Y, the amino acid substitution Trp^{15} to Tyr^{15}; L38M, the amino acid substitution Leu^{38} to Met^{38}; DesAc, no N-terminal acetyl group on polypeptide; Gdn-HCl, guanidine hydrochloride; TFA, trifluoroacetic acid; NATA, *N*-acetyltryptophanamide; NATyA, *N*-acetyltyrosinamide; CD, circular dichroism; Q, extent of fluorescence quenching; MW, molecular weight.

10.1021/bi0160718 CCC: $22.00
Published on Web 03/03/2002

The effect of the substitution L38M in the internal cavity of $(A\alpha_2)_2$ on anesthetic binding affinity has also been investigated (*14*). This substitution increased the binding affinity of halothane approximately 3.5-fold (i.e., $K_d = 200$ μM). Although the side chain of methionine is similar in relative volume, helix-forming propensity, and overall hydrophobicity to that of leucine, the more polarizable sulfur atom of methionine permits a more favorable interaction between $(A\alpha_2)_2$ and bound anesthetic (*14*). Additionally, the side chain of methionine is more flexible than that of leucine. Therefore, anesthetics are likely to be better accommodated in the internal cavity of the methionine-containing four-α-helix bundle.

The importance of aromatic side chains in anesthetic binding by proteins was investigated in the study described here. Specifically, the effect of the substitution W15Y on the structure and anesthetic binding affinity of the earlier $(A\alpha_2$-L38M$)_2$ four-α-helix bundle was examined. Residue[15] is located halfway along the length of α helices I and III at a hydrophobic *a* position of the heptad repeat. A tryptophan-to-tyrosine substitution at this position may modulate the strength of dipole−aromatic quadrupole interactions, a recently identified class of interaction in proteins (*16*, *17*) and, thus, affect anesthetic binding affinity. This substitution may thus give an indication of the importance of this type of interaction for anesthetic binding by proteins.

Additionally, reducing the size of a side chain at position 15 in the internal cavity of $(A\alpha_2$-L38M$)_2$ has the potential to either increase the size of this cavity or cause the α-helix bundle to collapse in on the cavity. Both of these structural changes might also influence anesthetic binding affinity by altering the volume and spatial features of the pre-existing cavity.

Substituting tyrosine in place of tryptophan still allows $(A\alpha_2)_2$ concentrations to be determined using UV spectroscopy, and anesthetic binding can be studied by following changes in the extents of fluorescence quenching using an existing procedure (*18*). To corroborate the results obtained for halothane, the binding of the anesthetic chloroform to the four-α-helix bundle $(A\alpha_2$-L38M/W15Y$)_2$ was also investigated.

MATERIALS AND METHODS

Materials. 9-Fluorenylmethoxycarbonyl (Fmoc)-protected amino acids and all reagents required for peptide synthesis were purchased from Perkin-Elmer Applied Biosystems (Foster City, CA). Acetonitrile was from Fisher Scientific (Pittsburgh, PA). Ethane dithiol was obtained from Fluka (Buchs, Switzerland). Halothane (2-bromo-2-chloro-1,1,1-trifluoroethane) was from Halocarbon Laboratories (Hackensack, NJ). The thymol preservative present in this commercial sample was removed by alumina column chromatography (*19*). All other chemicals were of reagent grade or better and obtained from the Sigma Aldrich Chemical Co. (St. Louis, MO).

Peptide Synthesis and Purification. The peptide was assembled as the C-terminal carboxyamide on a 0.25 mM scale using (Fmoc) amino acids and Fmoc 2,4-dimethoxybenzhydrylamide resin on an Applied Biosystems model 433A (Perkin-Elmer) solid-phase peptide synthesizer. Standard coupling conditions with 2-(1*H*-benzotriazol-1-yl)-1,1,3,3-tetramethyluronium hexafluorophosphate, 1-hydroxybenzotriazole, and *N*,*N*-diisopropylethylamine in *N*-methylpyrrolidone (NMP) and a 4-fold molar excess of amino acid were used throughout. The resin was washed with NMP and dichloromethane (DCM), and N-terminus acetylation was performed with acetic anhydride/pyridine (1:1 by volume). The acetylated peptide was again washed with NMP and DCM and cleaved from the resin, and the protecting groups were removed for 240 min in 2,2,2-trifluoroacetic acid (TFA)/ethanedithiol/water (90:8:2 by volume). Reversed-phase C_{18} high-performance liquid chromatography with aqueous acetonitrile gradients (40% (v/v) to 60% (v/v) over 60 min) containing 0.1% (v/v) TFA was used to purify crude peptides to homogeneity. Peptide identities were confirmed with laser desorption mass spectrometry. Solution molecular weights were determined by gel filtration on a Toso Haas G2000SW column (Montgomeryville, PA) using the following molecular weights standards: blue dextran (2 000 000 Da), bovine serum albumin (66 000 Da), carbonic anhydrase (29 000 Da), cytochrome *c* (12 400 Da), aprotinin (6500 Da), and cyanocobalamin (vitamin B_{12}; 1355 Da).

Circular Dichroism Spectroscopy. Spectra were recorded on a model 62 DS spectropolarimeter (Aviv, Lakewood, NJ) using 2 mm path-length quartz cells, a bandwidth of 1.0 nm, a scan step of 0.5 nm, and a time constant of 3.0 s. The buffer was 10 mM sodium phosphate (pH 7.0). The cell holder was maintained at 25.0 ± 0.1 °C.

Denaturation Studies. Denaturation of $(A\alpha_2$-L38M/W15Y$)_2$ was examined using circular dichroism (CD) spectroscopy, monitoring mean residue ellipticity at 222 nm (θ_{222}) as described earlier (*15*). The measured θ_{222} as a function of the added guanidine hydrochloride (Gdn-HCl) concentration was fit to an equation describing the unfolding of a dimeric four-α-helix bundle (*20*), using a nonlinear least-squares routine

$$\text{fraction folded} = 1 - [[\exp(\Delta G^{H_2O} + m[\text{denaturant}])]/RT]/[4P(1 + (8P/(\exp(\Delta G^{H_2O} + m[\text{denaturant}])/RT)) - 1)^{1/2}] \quad (1)$$

where ΔG^{H_2O} is the conformational stability of the protein, m is the slope of the unfolding transition, [denaturant] is the molar concentration of the Gdn-HCl, R is the gas constant, T is the absolute temperature, and P is the molar monomer concentration of $(A\alpha_2$-L38M/W15Y$)_2$.

Ligand Binding Measurements. The binding of the anesthetics halothane and chloroform to $(A\alpha_2$-L38M/W15Y$)_2$ was measured by following the change in tyrosine fluorescence intensity as ligand-free species was titrated with increasing amounts of ligand-equilibrated species. $(A\alpha_2$-L38M/W15Y$)_2$ was prepared in 20 mM sodium phosphate buffer and 130 mM NaCl (pH 7.0). After filtration (0.22 μm cutoff), concentrations were determined on a Cary 300 Bio UV−vis spectrophotometer (Florham Park, NJ) using $\epsilon = 1400$ M^{-1} cm^{-1} (*21*). Stock solutions (typically, 150 μM) were then diluted to the 2 μM used in titrations. The ligand-equilibrated $(A\alpha_2$-L38M/W15Y$)_2$ was prepared by introducing volumes of halothane or chloroform into gastight Hamilton syringes (Reno, NV) containing 2 μM $(A\alpha_2$-L38M/W15Y$)_2$ to final concentrations of 10 mM halothane and 35 mM chloroform and mixing for 1 h. The intermediate anesthetic concentra-

tions were obtained by mixing apo and anesthetic-equilibrated samples to give the final concentrations indicated in the figures.

Tyrosine fluorescence emission spectra, for solutions in a tightly stoppered 1 cm path-length quartz cell, were obtained on a Shimadzu model RF 5301 fluorescence spectrophotometer (Columbia, MD) by exciting at 275 nm (1.5 nm excitation bandwidth) and recording over the appropriate emission wavelength range (emission bandwidth 10.0 nm).

The extent of quenching (Q) observed is a function of the maximum possible quenching (Q_{max}) at infinite anesthetic concentration and the affinity of the anesthetic for the binding site on the four-α-helix bundle (K_d; *14*, *15*, *18*, *22*) close to the tyrosine side chains of $(A\alpha_2\text{-}l38M/W15Y)_2$

$$Q = (Q_{max}[\text{anesthetic}])/(K_d + [\text{anesthetic}]) \qquad (2)$$

Values for K_{SV} were calculated from Stern−Volmer plots (F_o/F vs [anesthetic]), where K_{SV} = slope, F_0 is the unquenched fluorescence intensity, and F is the fluorescence intensity at a given anesthetic concentration for the model fluorophores *N*-acetyltryptophanamide (NATA) and *N*-acetyltyrosinamide (NATyA).

pH Titrations. The deprotonation of tyrosine to form tyrosinate in $(A\alpha_2\text{-L38M/W15Y})_2$ was examined by following the shift in absorbance λ_{max} of $(A\alpha_2\text{-L38M/W15Y})_2$ solutions from 275 nm (tyrosine) to 293 nm (tyrosinate) as the pH was increased. The absorption spectrum of $(A\alpha_2\text{-L38M/W15Y})_2$ at 30 μM in 20 mM sodium phosphate buffer and 130 mM NaCl (pH 6.7) was recorded and then measured after each addition of NaOH. Values for pH were determined using a PHR-146 solid-state microcombination pH electrode (Lazar Research Laboratories, Inc., Los Angeles, CA) and a model 611 log *R* pH meter (Orion Research, Beverly, MA). The pK_a of the tyrosine hydroxyl was taken to be the point of inflection of the sigmoidal plots of proportion tyrosinate (A_{293}/A_{293}(final)) versus pH. The pK_a value obtained for tyrosine in $(A\alpha_2\text{-L38M/W15Y})_2$ was compared to those obtained in control titrations of NATyA and L-tyrosine, for which pK_a values are known.

The disappearance of tyrosine with increasing pH was also examined by following the decrease in the intensity of tyrosine fluorescence (λ_{ex} = 275 nm, λ_{em} = 305). Emission intensity data were treated in a manner similar to that described previously to obtain the pK_a value.

RESULTS

Four-α-Helix Bundle Design. The peptide $A\alpha_2$-L38M/W15Y was designed to fold and dimerize to form a water-soluble four-α-helix bundle with a hydrophobic core. This structure is based on earlier designs (*11*−*13*) and is shown schematically in Figure 1. Briefly, $(A\alpha_2\text{-L38M/W15Y})_2$ consists of two 62-residue di-α-helical polypeptide chains that each form a helix-turn-helix motif, then dimerize, in an antiparallel manner, to form the four-α-helix bundle. Each polypeptide chain contains two 27-residue amphipathic α-helical segments and an eight-residue flexible glycine linker.

Tyrosine[15] residues, at heptad position *a*, are located in the middle of helices I and III in the hydrophobic core of the dimer. The replacement of tryptophan with tyrosine at this position may affect the size of the internal cavity of the dimer and may also alter the overall energetics of anesthetic binding through a change in the strength of dipole−aromatic quadrupole interactions (see introduction).

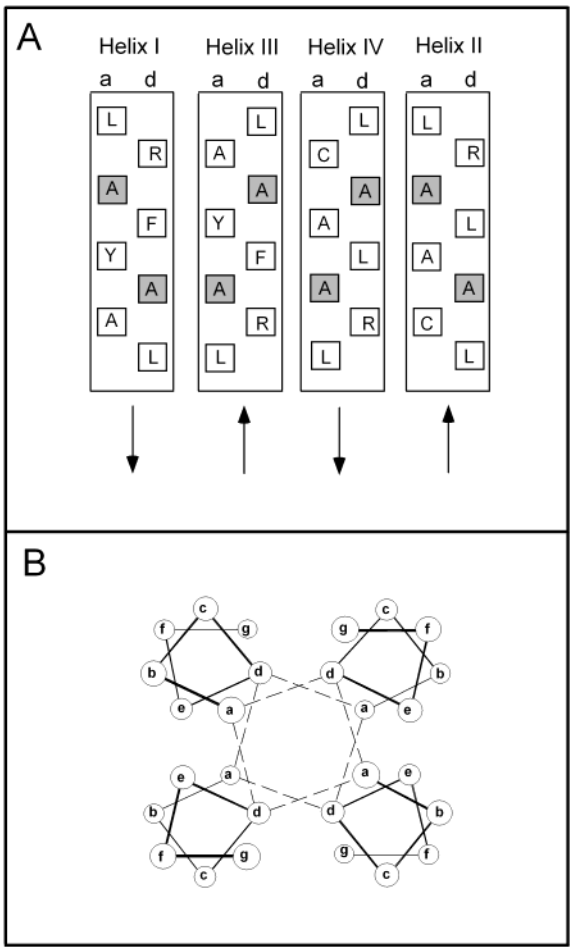

FIGURE 1: Representations of the structure of $(A\alpha_2\text{-L38M/W15Y})_2$. (A) Orientation of the α helices showing the side chains at the hydrophobic heptad postions *a* and *d*. The alanine residues that form the anesthetic binding cavity are shaded. (B) α-Helical wheel diagram, where α helices I and IV are antiparallel to II and III. The lower case italic letters denote the heptad positons. The dashed lines represent the interactions between side chains in the hydrophobic core. (Modified from ref *44*.)

α-Helical Content and Oligomeric State. Far-UV CD spectroscopy was used to demonstrate that, in 10 mM sodium phosphate buffer (pH 7.0), $(A\alpha_2\text{-L38M/W15Y})_2$ folds to give a structure that is predominantly α-helical. The spectrum in Figure 2 is very similar to that of poly(L-lysine) in an all-α-helical conformation (*23*). For a polypeptide chain of 62 residues, of which 54 are predicted to reside in α-helical structure, the value for mean residue ellipticity at 222 nm ($[\theta]_{222}$) should be −32 563 deg cm^2 dmol^{-1} (*24*). Experimentally, a value of −22 684 deg cm^2 dmol^{-1} for $[\theta]_{222}$ was obtained, so each polypeptide chain of $(A\alpha_2\text{-L38M/W15Y})_2$ is 70% α-helical. The experimentally determined $[\theta]_{222}$ value for this four-α-helix bundle is similar to those for other $(A\alpha_2)_2$ species (*14*) shown in Table 1, and the proportion of α-helical structure is similar to the proportions for α_3D (68.5% α-helix; *25*) and the three-α-helix bundle α_3-1 (80.5%; *15*) and deoxymyoglobin (73.0%; *26*). For $(A\alpha_2\text{-L38M/W15Y})_2$ in 10 mM sodium phosphate buffer (pH 7.0), the ratio $[\theta]_{222}/[\theta]_{208}$ is 1.005, suggesting that the four α-helices interact (*27*, *28*), consistent with an α-helix bundle

Table 1: Spectral and Thermodynamic Properties of $(A\alpha_2)_2$ Four-α-Helix Bundles

four-α-helix bundle	solution M_r (kDa)	fluorescence emission λ_{max} (nm)	$[\theta]_{222}$ (deg cm^2 dmol^{-1})	ΔG^{H_2O} (kcal/mol)	m (kcal/mol M)	anesthetic K_d (μM)[a]
$(A\alpha_2$-L38M/W15Y$)_2$	19.9	305	−22 600	−13.1 ± 0.2	2.6 ± 0.1	1200 ± 90 *4100 ± 90*
$(A\alpha_2$-L38M$)_2$[b]	14.9	323	−22 000	−13.9 ± 0.2	2.0 ± 0.1	*1400 ± 200*
(DesAc-$A\alpha_2$-L38M$)_2$[c]	14.9	323	−21 600	−11.7 ± 0.2	2.0 ± 0.1	200 ± 10
$(A\alpha_2)_2$[c]	18.5	327	−23 000	−14.3 ± 0.8	2.0 ± 0.1	710 ± 40
(DesAc-$A\alpha_2)_2$[c]	13.2	327	−22 000	−11.5 ± 0.3	1.8 ± 0.1	690 ± 60

[a] Regular text for halothane, italic type for chloroform. DesAc denotes no N-terminus acetyl group. [b] Reference *43*. [c] Reference *14*.

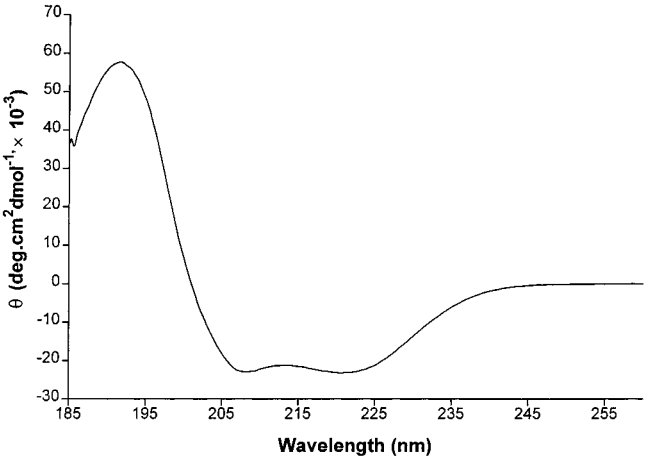

FIGURE 2: Far-UV CD spectrum of $(A\alpha_2$-L38M/W15Y$)_2$ at 10 μM under nondenaturing conditions (10 mM sodium phosphate buffer (pH 7.0)).

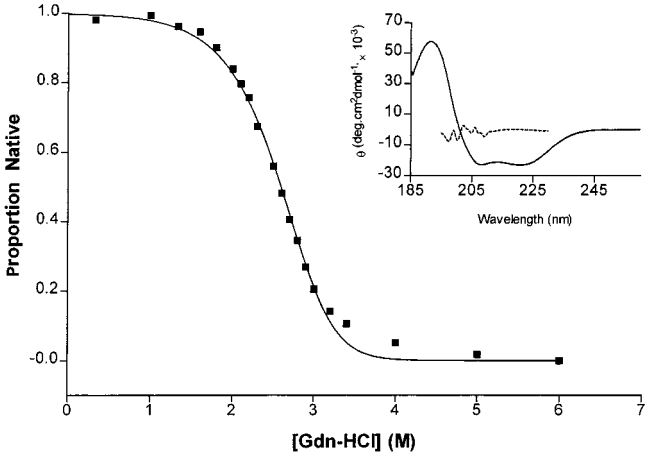

FIGURE 3: Guanidine hydrochloride-induced unfolding of $(A\alpha_2$-L38M/W15Y$)_2$ as monitored by circular dichroism spectroscopy at 222 nm (10 μM $(A\alpha_2$-L38M/W15Y$)_2$, in 10 mM sodium phosphate buffer (pH 7.0)): (inset) the far-UV CD spectrum of $(A\alpha_2$-L38M/W15Y$)_2$ in the absence (—) and presence (---) of 5 M guanidine hydrochloride.

structure. Gel filtration analysis confirmed that the predominant species in preparations of $(A\alpha_2$-L38M/W15Y$)_2$ was indeed one with a MW consistent with a dimer (Table 1).

Denaturation Studies. The conformational stability of $(A\alpha_2$-L38M/W15Y$)_2$ was determined by following the change in α-helical CD ($[\theta]_{222}$) as a function of increasing guanidine hydrochloride concentration. Figure 3 (inset) shows that $(A\alpha_2$-L38M/W15Y$)_2$ undergoes a large change in $[\theta]_{222}$ in the presence of this chaotrope that is consistent with a loss of α-helical structure.

When $[\theta]_{222}$ is plotted against guanidine hydrochloride concentration (Figure 3), the curve obtained is sigmoidal, and the sharpness of the transition shows that the loss of α helicity occurs as a two-state cooperative process, as determined previously for the $(A\alpha_2)_2$ four-α-helix bundles (*14*). The midpoint guanidine hydrochloride concentration for $(A\alpha_2$-L38M/W15Y$)_2$ is 2.5 ± 0.1 M, as compared to 2.1 ± 0.1 M for $(A\alpha_2$-L38M$)_2$ (*14*).

Values for ΔG^{H_2O} for the $(A\alpha_2)_2$ four-α-helix bundles are given in Table 1 and represent an extrapolation of the free energy of unfolding in the absence of guanidine hydrochloride (*29*). They are similar to the values reported by others for synthetic four-α-helix bundles (*30*−*33*). The ΔG^{H_2O} values (Table 1) for the $(A\alpha_2)_2$ four-α-helix bundles show that, for the deacetylated species, the substitution of leucine for methionine at position 38 has little effect on structural stability, although deacetylation itself results in a destabilization of 2.7 kcal/mol. Thus, a comparison of the ΔG^{H_2O} values for the original $(A\alpha_2)_2$ species (14.3 ± 0.8 kcal/mol) and $(A\alpha_2$-L38M/W15Y$)_2$ (13.1 ± 0.2 kcal/mol) is valid and shows that a small decrease in stability of 1.2 kcal/mol occurs as a consequence of W15Y substitution.

Binding of Volatile Anesthetics. The affinities of the anesthetics halothane and chloroform for the four-α-helix bundle $(A\alpha_2$-L38M/W15Y$)_2$ were determined by titrating one with the other and measuring the extents of tyrosine fluorescence quenching. The side chains of the two tyrosine residues of this four-α-helix bundle are presumed to reside in the hydrophobic cavity of the four-α-helix bundle, as is the case for the earlier tryptophan-containing $(A\alpha_2)_2$ species (*14*). Therefore, if anesthetics bind in the central cavity of $(A\alpha_2$-L38M/W15Y$)_2$, it is predicted that tyrosine fluorescence will be quenched, thus providing a measure of the extent of anesthetic binding.

Tyrosine fluorescence emission spectra are shown in parts A and B of Figure 4 (insets) and indicate that, in the presence of 10 mM halothane and 35 mM chloroform, tyrosine fluorescence is quenched substantially. From the binding curves in parts A and B of Figure 4, it was determined that halothane bound to the $(A\alpha_2$-L38M/W15Y$)_2$ bundle with a K_d of 1200 ± 100 μM to give a Q_{max} (the maximum extent of fluorescence quenching) of 0.93 ± 0.04.

Chloroform bound with a K_d of 4100 ± 100 μM and gave a Q_{max} of 1.01 ± 0.01.

Parts A and B of Figure 4 also show that the extent of quenching of $(A\alpha_2$-L38M/W15Y$)_2$ tyrosine fluorescence by halothane and chloroform is approximately 20-fold lower in the presence of 6.0 M Gdn-HCl than in the absence of this chaotrope (extrapolation to anesthetic concentrations that would give 50% quenching). The more efficient quenching seen in the absence of Gdn-HCl is consistent with the

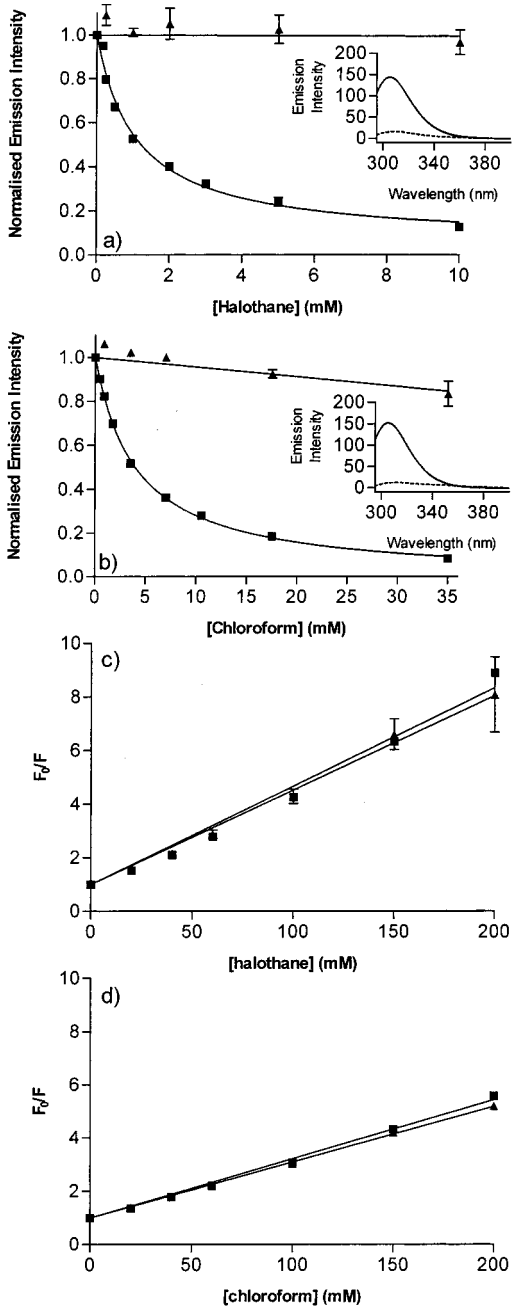

FIGURE 4: Binding of halothane (A) and chloroform (B) to $(A\alpha_2\text{-L38M/W15Y})_2$ as monitored by progressive tyrosine fluorescence quenching in 20 mM phosphate buffer and 130 mM NaCl (pH 7.0) (■) and the same buffer with 6.0 M Gdn-HCl (▲). The helix bundle concentration was 2 μM. The λ_{ex} was 275 nm, and the emission λ_{max} was 305 nm. Data points are the means of three replicate experiments, and the error bars represent the SD. The lines are a fit to eq 2, as per ref *13*. The insert in A shows the tyrosine fluorescence emission spectrum of $(A\alpha_2\text{-L38M/W15Y})_2$ in the absence (—) and presence (---) of 10 mM halothane, while that in B shows $(A\alpha_2\text{-L38M/W15Y})_2$ in the absence (—) and presence (---) of 35 mM chloroform. Panel C shows Stern−Volmer plots for the interaction of halothane with *N*-acetyltryptophanamide (NATA (■), $K_{SV} = 25 \pm 1\ M^{-1}$) and NATyA ((▲) $K_{SV} = 27 \pm 4\ M^{-1}$). The interactions of chloroform with NATA ((■) $K_{SV} = 43 \pm 1\ M^{-1}$) and NATyA ((▲) $K_{SV} = 47 \pm 2\ M^{-1}$) are shown in panel D. Values for K_{SV} were determined by fitting the data to the equation

$$F_0/F = 1 + K_{SV}[\text{Anesthetic}] \quad (3)$$

retention of anesthetic in close proximity to tyrosine, which would occur if the anesthetic were bound in the interior of

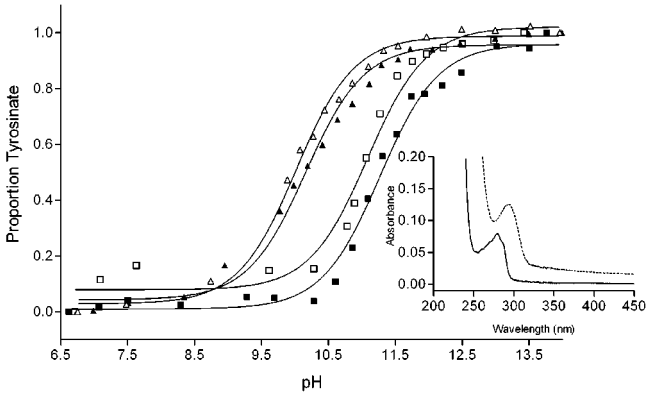

FIGURE 5: pH titration curves for tyrosine phenol groups. Those for tyrosine in $(A\alpha_2\text{-L38M/W15Y})_2$ (■) or as free L-tyrosine (▲) and NATyA (△) were obtained by monitoring changes in A_{293} (λ_{max} of tyrosinate). The curve (□) was obtained from tyrosine fluorescence data, where it was assumed that the tyrosine emission intensity at a given pH value can be used to calculate the ratio tyrosine/tyrosinate. The $(A\alpha_2\text{-L38M/W15Y})_2$ solutions were 35 μM, while those of L-tyrosine and NATyA were 70 μM, all in 20 mM sodium phosphate buffer and 130 mM NaCl and an initial pH of 6.7. Data were fit to a sigmoid function, the point of inflection of which represents the pK_a of the titratable hydroxyl group: (inset) the absorption spectrum of $(A\alpha_2\text{-L38M/W15Y})_2$ at pH 6.6 (—) and 12.0 (---).

a four-α-helix bundle structure. The minimal quenching of helix bundle tyrosine fluorescence by halothane and chloroform seen in the presence of Gdn-HCl is consistent with an aqueous collisional fluorescence quenching mechanism. In 6.0 M Gdn-HCl, the four-α-helix bundle is unfolded (Figure 4), the internal anesthetic binding site is lost, and the tyrosine side chains are solvent-exposed.

The K_d values in Table 1 suggest that the $(A\alpha_2)_2$ four-α-helix bundle containing tryptophan binds halothane approximately 6 times more tightly than $(A\alpha_2\text{-L38M/W15Y})_2$. Chloroform was bound approximately 3 times more tightly to $(A\alpha_2\text{-L38M})_2$ than to $(A\alpha_2\text{-L38M/W15Y})_2$. These differences are difficult to explain in terms of a dissimilarity in the extent to which these anesthetics quench tryptophan and tyrosine fluorescence. The control titrations in Figure 4C for halothane with *N*-acetyltryptophanamide (NATA) and NATyA show that the fluorescence of both amino acid derivatives is quenched to essentially the same extent, suggesting a similar quenching mechanism for both aromatic ring systems. Figure 4D suggests that the same is true for indole and phenol quenching by chloroform. Thus, the differences in the K_d values for the binding of halothane or chloroform to the tyrosine- and tryptophan-containing four-α-helix bundles, calculated from fluorescence quenching data, reflect energetically more favorable interactions with tryptophan as compared to tyrosine.

pH Titrations. Further evidence that the two equivalent tyrosines of $(A\alpha_2\text{-L38M/W15Y})_2$ are solvent-inaccessible was obtained through the determination of the pK_a of the hydroxyl group of this side chain. If tyrosine side chains reside in the hydrophobic interior of dimeric structures, then the pK_a of the hydroxyl group should be greater than 10.1, the value for solvent-exposed tyrosine (*34*). Figure 5 shows how the proportion of tyrosinate in solutions of $(A\alpha_2\text{-L38M/W15Y})_2$, NATyA, and L-tyrosine vary with pH. The pK_a values, taken to be the point of inflection for a particular plot, were 10.16 ± 0.05 for L-tyrosine and 10.02 ± 0.04 for

NATyA (Figure 5), consistent with earlier studies (*34*, *35*). The pK_a of Y^{15} in $(A\alpha_2\text{-L38M/W15Y})_2$ was determined to be 11.36 ± 0.07, in agreement with the value of 11.3 for a tyrosine buried in the hydrophobic core of a three-α-helix bundle (*35*). This high value corroborates the conclusion that the side chain of Y^{15} is located in a solvent-inaccessible and hydrophobic environment.

The pK_a of the Y^{15} hydroxyl group in $(A\alpha_2\text{-L38M/W15Y})_2$ was also determined by following the decrease in tyrosine fluorescence intensity with increasing pH. Because tyrosinate is nonfluorescent (*36*), it is possible, given the initial tyrosine fluorescence intensity, to relate the intensity remaining at a given pH value to the ratio of tyrosine/tyrosinate. Using this approach, a pK_a value of 11.09 ± 0.07 was obtained, consistent with that obtained from A_{293} data. A similar approach could not, however, be used to corroborate this pK_a value using tyrosine absorption data (i.e., A_{275} values) because tyrosinate also absorbs appreciably at 275 nm (Figure 5).

DISCUSSION

In the present study, the effect of reducing the size of an aromatic side chain that packs into the interior of a synthetic four-α-helix bundle was examined. We found that the substitution W15Y did not effect the overall secondary structure of the $(A\alpha_2)_2$ four-α-helix bundle. With tyrosine at position 15, the four-α-helix bundle contains a similar amount of α helix as it does with tryptophan and the side chain of residue[15] still resides in the internal hydrophobic cavity. Additionally, the stability of $(A\alpha_2)_2$ was only decreased by approximately 1 kcal/mol as a consequence of W15Y substitution.

The decrease in the stability of $(A\alpha_2)_2$ caused by W15Y substitution can be explained in terms of the hydrophobic effect. Tyrosine is less hydrophobic than tryptophan (*37*, *38*) and should therefore be easier to transfer from the interior of the four-α-helix bundle to the solvent. Furthermore, the decrease in stability of $(A\alpha_2)_2$ caused by W15Y substitution is consistent with the lower α-helical propensity of tyrosine as compared to tryptophan (*30*).

The plots in Figure 4 show that the extent of quenching seen when halothane or chloroform are mixed with $(A\alpha_2\text{-L38M/W15Y})_2$ in the presence of 6.0 M Gdn-HCl is approximately 20-fold less than that seen in the absence of this chaotrope. This suggests that these anesthetics are retained in close proximity to the tyrosine side chains in the internal cavity of folded $(A\alpha_2\text{-L38M/W15Y})_2$. Following from this, it appears that the binding of halothane and chloroform has little effect on the native structure of $(A\alpha_2\text{-L38M/W15Y})_2$. In the presence of 6.0 M Gdn-HCl, the four-α-helix bundle is unfolded, and the side chains of tyrosine would be solvent-exposed. Thus, the extent of quenching is less because it occurs primarily by a less efficient collision-controlled mechanism, producing titration results more akin to those seen for NATyA (Figure 4C). The assumption that anesthetics bind in close proximity to the Y^{15} resides is consistent with earlier photolabeling results (*14*).

Unlike tryptophan, the fluorescence λ_{max} of tyrosine shows little dependence on environmental polarity. Thus, an examination of emission λ_{max} values offers little additional insight into whether the structure of $(A\alpha_2\text{-L38M/W15Y})_2$ is altered appreciably as a consequence of anesthetic binding. Earlier results (*14*), however, suggest that a structural change in $(A\alpha_2)_2$ four-α-helix bundles is minimal because only small shifts in tryptophan emission λ_{max} were observed upon anesthetic binding.

All of the K_d values for halothane presented in Table 1 compare favorably with the EC_{50} value for this anesthetic in humans (250 μM; *1*). Similarly, the EC_{50} for chloroform in dogs is 1.2 mM (*39*). This suggests that the structure of the internal cavity of the four-α-helix bundles is a good approximation for the in vivo anesthetic receptors.

The substitution W15Y was found to affect anesthetic binding affinity, resulting in 6-fold and 3-fold decreases in the K_d for halothane and chloroform binding, respectively. Control titration data do not suggest that this difference reflects an artifact, for example, a dissimilarity in the fluorescence quenching mechanisms for tryptophan and tyrosine ring systems. Therefore, it is concluded that the affinities of halothane and chloroform for the tyrosine-containing four-α-helix bundle is indeed less than that for the tryptophan-containing analogue.

The quenching of tyrosine and tryptophan fluorescence by halothane and chloroform probably occurs as a consequence of an increase in electron spin intersystem crossing rates. This is caused by spin−orbital coupling between the excited singlet state of the aromatic ring(s) and the heavy atoms chlorine and bromine (*40*). Intersystem crossing occurs when electrons in the fluorophore are converted from the first excited singlet state (S_1) to the first excited triplet state (T_1). The subsequent relaxation from T_1 to S_0 is spin-forbidden and occurs via the process of phosphorescence, which is characterized by the emission of photons at longer wavelengths and over longer periods than that which occurs via fluorescence (S_1 to S_0; *40*). Thus, intersystem crossing and subsequent relaxation via phosphorescence results in fluorescence quenching.

The effect of W15Y substitution on halothane and chloroform binding affinities may be explained in terms of these anesthetics fitting more "snuggly" in the internal cavity of the tryptophan-containing four-α-helix bundle, forming more favorable interactions with the side chains therein. In the case of the tyrosine-containing analogue, the internal cavity may be larger, and bound anesthetic may therefore exhibit greater rotational and translational freedom. This would shorten the average time the anesthetics spend engaged in favorable interactions with side chains such as that of Y^{15}, in turn diminishing the extent of fluorescence quenching. This is consistent with the conclusion that these anesthetics are bound less tightly to the tyrosine-containing four-α-helix bundle than to the tryptophan-containing analogue.

Alternatively, the observed differences in affinities of halothane and chloroform for the tryptophan- and tyrosine-containing four-α-helix bundles reflect differences in the strengths of dipole−aromatic quadrupole interactions. In addition to their dipole moment, the aromatic ring systems indole and phenol possess a strong quadrupole moment. This is created by the permanent nonspherical distribution of electrons in the delocalized clouds, which are most dense above and below the plane of the ring system, as well as the radially symmetric C−H dipoles (*16*, *17*). As a result, aromatic ring systems bind cations and acidic hydrogens with

surprisingly high affinity. For example, in the gaseous phase, the interaction between K^+ and benzene is 1 kcal/mol more favorable than the interaction between K^+ and water (*41*). In biological systems, the charged guanidino group of arginine is seen to stack directly over the center of aromatic side chains with surprising frequency (*42*). From these observations, it has been suggested that in the interiors of proteins the side chains of tryptophan, tyrosine, and phenylalanine act as "hydrophobic anions" (*16*). Thus, in the case of the $(A\alpha_2)_2$ four-α-helix bundles, dipole−aromatic quadrupole interactions may contribute to the energetics of anesthetic binding, which although formally uncharged, do possess permanent dipole moments and can therefore bind with higher affinity to the tryptophan-containing four-α-helix bundles because of the stronger dipole−aromatic quadrupole interactions afforded by the larger number of π electrons in the indole ring system. Thus, we conclude, from the comparison of results presented here with those of Johansson et al. (*14*) that the size of the aromatic ring system present in the ligand binding cavity of the four-α-helix bundles can have an appreciable effect on anesthetic binding affinity. This, in turn, suggests that dipole−aromatic quadrupole interactions can play a crucial role in how proteins bind ligands, substrates, and cofactors.

Table 1 shows that the difference between the K_d for the binding of halothane to $(A\alpha_2)_2$ and that $(DesAc\text{-}A\alpha_2)_2$ is within the limits of experimental error. Therefore, it is likely that the removal of the N-terminal acetyl group, which should weaken the strength of the α-helix dipole across $(A\alpha_2)_2$, has little effect on the binding affinity of halothane. Thus, the contribution of N-terminal acetylation to the observed differences in the affinity of halothane for $(DesAc\text{-}A\alpha_2\text{-}L38M)_2$ and $(A\alpha_2\text{-}L38M/W15Y)_2$ is likely to be negligible. Rather, as discussed previously, the difference is, instead, a reflection of a dissimilarity in internal cavity size or the strength of dipole−aromatic quadrupole interactions.

The study presented here illustrates that tyrosine fluorescence can be used to follow anesthetic binding to proteins and peptides. This technique shows no utility, however, in following protein denaturation because tyrosine fluorescence λ_{max} values show little dependence on environmental polarity. Information pertaining to the environment of tyrosine side chains in native structures can, nonetheless, be obtained by determining their pK_a values, as illustrated here.

SUMMARY

Substituting tryptophan for tyrosine in the interior of a synthetic four-α-helix bundle had little affect on its overall structure, the environment of the aromatic side chain, or the overall stability of the structure. Anesthetic binding affinity was, however, affected by W15Y substitution; the K_d values for halothane and chloroform binding were increased approximately 6- and 3-fold, respectively. This illustrates the importance of the role aromatic side chains play in the binding of anesthetics by four-α-helix bundles and implicates the presence of dipole−aromatic quadrupole interactions as being crucial in defining the binding affinity. This class of interaction may therefore prove to be more important than was previously thought in controlling ligand, substrate, and cofactor binding by proteins and enzymes.

ACKNOWLEDGMENT

Laser desorption mass spectrometry was performed by the Protein Chemistry Laboratory, 4 Stellar-Chance Building, University of Pennsylvania, Phildaelphia, PA 19104.

REFERENCES

1. Franks, N. P., and Lieb, W. R. (1994) *Nature 367*, 607−614.
2. Eckenhoff, R. G., and Johansson, J. S. (1997) *Pharmacol. Rev. 49*, 343−367.
3. Ueda, I., and Kamaya, H. (1973) *Anesthesiology 38*, 425−436.
4. Eckenhoff, R. G., Tanner, J. W., and Liebman, P. A. (2001) *Proteins 42*, 436−441.
5. Harris, R. A., Mihic, S. J., Dildy-Mayfield, J. E., and Machu, T. K. (1995) *FASEB J. 9*, 1454−1462.
6. Grutter, T., and Changeaux, J.-P. (2001) *Trends Biochem. Sci. 26*, 459−463.
7. Xu, Y., Seto, T., Tang, P., and Firestone, L. (2000) *Biophys. J. 78*, 746−751.
8. Ishizawa, Y., Sharp, R., Liebman, P. A., and Eckenhoff, R. G. (2000) *Biochemistry 39*, 8407−8502.
9. Doyle, D. A., Cabral, J. M., Pfuetzner, R. A., Kuo, A., Gulbis, J. M., Cohen, S. L., Chait, B. T., and MacKinnon, R. (1998) *Science* 280, 69−77.
10. Rees, D. C., Komiya, H., Yeates, T. O., Allen, J. P., and Feher, G. (1989) *Annu. Rev. Biochem. 58*, 607−633.
11. Gibney, B. R., Mulholland, S. E., Rabanal, F., Skalicky, J. J., Wand, A. J., and Dutton, P. L. (1996) *Proc. Natl. Acad. Sci. U.S.A. 93*, 15041−15046.
12. Gibney, B. R., Johansson, J. S., Rabanal, F., Skalicky, J. J., Wand, A. J., and Dutton, P. L. (1997) *Biochemistry 36*, 2798−2806.
13. Gibney, B. R., Rabanal, F., Skalicky, J. J. Wand, A. J., and Dutton, P. L. (1997) *J. Am. Chem. Soc. 119*, 2323−2324.
14. Johansson, J. S., Scharf, D., Davies, L. A., Reddy, K. S., and Eckenhoff, R. G. (2000) *Biophys. J. 78*, 982−993.
15. Johansson, J. S., Gibney, B. R., Rabanal, F., Reddy, K. S., and Dutton, P. L. (1998) *Biochemistry 37*, 1422−1429.
16. Dougherty, D. A. (1996) *Science 271*, 163−168.
17. Gallivan, J. P., and Dougherty, D. A. (1999) *Proc. Natl. Acad. Sci. U.S.A. 96*, 9459−9464.
18. Johansson, J. S., Eckenhoff, R. G., and Dutton, P. L. (1995) *Anesthesiology 83*, 316−325.
19. Shibata, A., Morita, K., Yamashita, T., Kamaya, H., and Ueda, I. (1991) *J. Pharm. Sci. 80*, 1037−1041.
20. Mok, Y.-K., De Prat Gay, G., Butler, J. P., and Bycroft, M. (1996) *Protein Sci. 5*, 310−319.
21. Freifelder, D. (1982) in *Physical Biochemistry*, p 501, W.H. Freeman and Co., New York.
22. Johansson, J. S., Rabanal, F., and Dutton, P. L. (1996) *J. Pharmacol. Exp. Ther. 279*, 56−61.
23. Brahms, S., and Brahms, J. (1980) *J. Mol. Biol. 138*, 149−178.
24. Chan, Y.-H., Yand, J. T., and Chau, K. H. (1974) *Biochemistry 13*, 3350−3359.
25. Walsh, S. T. R., Cheng, H., Bryson, J. W., Roder, H., and DeGrado, W. F. (1999) *Proc. Natl. Acad. Sci., U.S.A. 96*, 5486−5491.
26. Takano, N. (1977) *J. Mol. Biol. 110*, 569−584.
27. Lau, S. Y. M., Taneja, A. K., and Hodges, R. S. (1984) *J. Biol. Chem.* 259, 13253−13261.
28. Cooper, T. M., and Woody, R. W. (1990) *Biopolymers 30*, 657−676.
29. Pace, C. N. (1986) *Methods Enzymol. 131*, 266−280.
30. O'Neil, K. T., and DeGrado, W. F. (1990) *Science 250*, 646−651.
31. Handel, T. M., Williams, S. A., Menyhard, D., and DeGrado, W. F. (1993) *J. Am. Chem. Soc. 115*, 4457−4460.
32. Handel, T. M., Williams, S. A., and DeGrado, W. F. (1993) *Science 261*, 879−885.

33. Betz, S. F., and DeGrado, W. F. (1996) *Biochemistry 35*, 6955−6962.
34. Lehninger, A. L. (1982) *Principles of Biochemistry*, p 107, Worth Publishers, Inc., New York.
35. Tommos, C., Skalicky, J. J., Pilloud, D. L., Wand, A. J., and Dutton, P. L. (1999) *Biochemistry 38*, 9495−9507.
36. Creed, D. (1984) *Photochem. Photobiol. 39*, 563−575.
37. Rose, G. D., Geselowitz, A. R., Lesser, G. J., Lee, R. H., and Zehfus, M. H. (1985) *Science 229*, 834−838.
38. Wimley, W. C., and White, S. H. (1996) *Nat. Struct. Biol. 3*, 842−848.
39. Eger, E. I., Lundgren, C., Miller, S., and Stevens, W. C. (1969) *Anesthesiology 30*, 129−135.
40. Lakowicz, J. R. (1999) *Principles of Fluorescence Spectroscopy*, pp 5−6, Kluwer Academic/Plenum Publishers, New York.
41. Sunner, J., Nishizawa, K., and Kebarle, P. (1981) *J. Phys. Chem. 85*, 1814−1820.
42. Flocco, M. M., and Mowbray, S. L. (1994) *J. Mol. Biol. 235*, 709−717.
43. Solt, K., and Johansson, J. S. (2000) *Biophys. J. 78*, 895A.
44. Betz, S. F., Liebman, P. A., and DeGrado, W. F. (1997) *Biochemistry 36*, 2450−2458.

BI0160718